

CALIBRATION OF A NUMERICAL MODEL FOR MASONRY INFILLED RC FRAMES

A. Stavridis¹ and P. B. Shing²

¹ Graduate Research Assistant, Dept. of Structural Engineering, University of California, San Diego, USA

² Professor, Dept. of Structural Engineering, University of California, San Diego, USA

Email: andreas@ucsd.edu, pshing@ucsd.edu

ABSTRACT :

This paper introduces a finite element scheme and a systematic calibration approach for masonry infilled RC frames. The modeling scheme combines the smeared crack approach with discrete crack elements to allow for the opening of diffused flexural and dominant shear cracks. It is, therefore, able to capture the nonlinear material behavior and the interaction of the infill wall with the bounding RC frame. The proposed modeling approach and calibration methodology are evaluated with experimental data of two non-ductile, infilled, RC frames with distinct failure mechanisms. The comparison of the numerical and laboratory data indicates that the numerical models successfully capture the highly nonlinear behavior of the physical specimens.

KEYWORDS: masonry, RC frame, finite elements

1. INTRODUCTION

Reinforced concrete (RC) frames with masonry infill walls can be frequently found in areas of high seismic risk around the world. Although infills can develop strong interaction with the bounding frames under seismic loads, they are often considered as non-structural elements and are overlooked in the structural analysis and design. The issue as to how infills affect the seismic performance of an RC building is intricate as the exact role of the masonry walls during an earthquake is complex and not yet clearly understood. The variability of material properties, geometric configurations and construction methods add to the complexity of this problem.

Evaluating the seismic performance of infilled frames has been a challenging task for structural engineers. ASCE 41-06 (2006) includes guidelines for simplified analytical methodologies, however, they are not satisfactory in terms of completeness and reliability, and have not been fully validated. The most powerful analysis tool is the nonlinear finite element modeling. Lotfi (1992) and Attard et al. (2007) modeled masonry walls with a combination of continuum elements and interface elements and Mehrabi and Shing (1994) simulated masonry infilled RC frames with a combination of discrete and smeared crack elements for the frame and the infill wall. Their models showed some success in capturing the nonlinear behavior of infilled frames but failed to capture some of the failure mechanisms observed in their tests due to issues related to the finite element discretization and model calibration. ASCE 41-06 recognizes the recent advancements in numerical simulations and permits the analysis of such structures with nonlinear finite element methods. Nevertheless, it does not provide further guidance to ensure the consistency of the analyses.

This paper presents a reliable methodology for the development and calibration of nonlinear finite element models to assess the seismic performance of masonry infilled RC frames. The finite element scheme combines the advantages of smeared and discrete crack modeling approaches to reproduce the different failure modes of infilled frames, including the mixed-mode fracture of mortar joints and shear failure of RC columns. The numerical results for two frames tested by Mehrabi et al. (1994) presented in this paper demonstrate that the proposed methodology can capture the actual performance of the laboratory specimens, and predict well their strength and post-peak behavior.

2. IN-PLANE BEHAVIOR OF INFILLED FRAMES

The seismic performance of masonry infilled RC frames has intrigued the interest of many researchers worldwide and has been the subject of a large number of experimental studies (Mehrabi et al. 1994 Fardis et al. 1999 and Al-Chaar et al. 2003). These studies indicate that the in-plane lateral resistance of an infilled frame is not equal to a simple summation of the resistance of the masonry wall and the bare frame. For low levels of lateral load, an infilled frame acts as a monolithic load-resisting system. As the load increases, the infill tends to partially separate from the frame and form a compression

strut mechanism. However, the compression strut may or may not evolve into a governing load resisting mechanism depending on the stiffness and strength of the infill with respect to those of the RC frame. Mehrabi et al. (1994) identified a range of failure mechanisms indicating the importance of the interaction of the RC frame and the infill wall. Therefore, a consistent modeling scheme and calibration approach is needed to capture this interaction.

3. FINITE ELEMENT MODELING SCHEME

The failure infilled RC frames may involve diffused flexural cracks and dominant shear cracks in RC members, tensile and shear fracture in mortar joints, and compressive failure of concrete and masonry units. These failure modes can be accurately captured if smeared-crack elements are supplemented with zero-thickness interface elements to model cracks in a discrete fashion, so that the inherent problems of smeared crack elements such as stress-locking can be alleviated and the sliding shear failure of masonry mortar joints can be modeled. A general modeling approach, applicable to complicated structures without prior knowledge of the actual failure mechanism, is considered here.

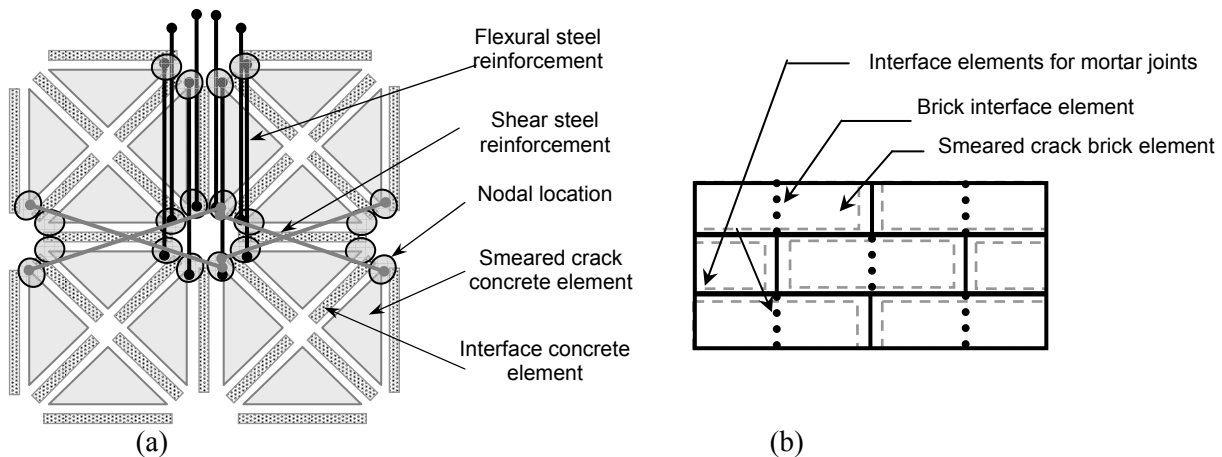


Figure 1: Finite element discretization (a) of RC members: mesh of concrete elements and flexural and shear reinforcement and (b) of masonry infill

3.1 Discretization scheme for reinforced concrete members

Reinforced concrete members are often discretized with a rectangular grid of nodes connected with quadrilateral smeared-crack elements. To model shear cracks in a discrete fashion without the prior knowledge of their locations and orientations, each quadrilateral element can be replaced with a module of smeared-crack and interface elements. Each module consists of four triangular smeared-crack elements connected with four, diagonally placed, double-noded, zero-thickness interface elements, as illustrated in Figure 1(a). Each module is connected to the adjacent modules with horizontal and vertical interface elements. With the proposed mesh topology, discrete cracks can develop at angles of 0° , 90° and $\pm \theta$, where θ can be close to 45° to represent shear cracks. The introduction of discrete cracks not only removes the undesired stress locking under shear but also alleviates the mesh-size sensitivity problem, which is well known for smeared-crack models (Bazant and Oh 1983). To model the nonlinear behavior of the member in a refined manner, the concrete members can be discretized with as many modules as needed in either direction to obtain an accurate solution. In general, it is desirable that the size of an element be close to the compressive failure zone in the concrete member.

With the aforementioned discretization scheme, each interior node of the initial orthogonal mesh is replaced by eight nodes, each associated with one triangular element and two interface elements. Consequently, the steel bars can be connected to the concrete elements in a number of ways. However, it is desirable to have as many nodes of a smeared-crack element connected to steel bars as possible to enhance numerical stability, while every potential discrete crack crosses the same quantity of steel as in reality.

A scheme has been proposed for the flexural and shear reinforcement in light of the above considerations. As illustrated in Figure 1a, the flexural steel at each interior location is equally divided to eight truss elements so that every triangular element is attached to flexural steel at two of its nodes. Along the external edges of the RC member there are four nodes at each location, therefore the flexural steel is divided into four truss elements. This arrangement provides a degree of restraint to the triangular elements when the tensile strength of the adjacent interface elements has been exhausted. For

the shear reinforcement, the number of parallel bars can be reduced for computational efficiency. However, the total shear steel area at each location can be divided in two bars placed in a zigzag pattern, as shown in Figure 1(a). These bars help to prevent unrealistic horizontal sliding along the concrete interface elements. With this modelling scheme, every potential horizontal and diagonal crack would cross the proper quantity of flexural and shear steel.

3.2 Modeling scheme for masonry infill

In a masonry assembly, the mortar is normally much weaker than the brick. The failure, however, may involve crushing and tensile fracturing of masonry units, fracturing of mortar joints, and tensile or shear fracturing in the interface between mortar joints and masonry units. When the masonry assembly is under compression, the lateral expansion of the mortar introduces a lateral tensile stress on the brick, which at the same time provides a confining stress on the mortar. This often leads to tensile splitting of the brick with cracks parallel to the compression force. Due to the brick-mortar interaction, the stiffness and compressive strength of the masonry assembly are lower than the brick but higher than the mortar.

For the modeling of a masonry wall, one can make a significant simplification and represent an entire mortar joint with a zero-thickness cohesive interface model (Lotfi and Shing 1994). In this case, the dimensions of the masonry units need to be modified in the finite element model to maintain the same overall dimensions of a masonry assembly as shown in Figure 1(b). Clearly, with this approach, the failure of a brick-mortar interface is not distinguished from that of the mortar layer itself, while the brick-mortar interaction and the tensile splitting of the brick units under compression can not be captured. With these considerations, it is evident that the properties of the continuum elements representing the brick should reflect those of a masonry assembly rather than those of the brick itself. This is discussed further in the calibration procedure in the following section. With the proposed discretization scheme, each masonry unit is modeled with two rectangular continuum elements that are inter-connected with a vertical interface element. The latter allows for the tensile splitting of the brick units and the relative sliding motion within a fractured unit.

4. CONSTITUTIVE MODELS

4.1 Smearred-crack model

The smeared-crack model used to simulate the nonlinear behavior of concrete and masonry in this study was originally developed by Lotfi and Shing (1991) and incorporated in the finite element analysis program FEAP (Taylor 2007). In this model, the tensile fracture is governed by a tension cutoff criterion, while the compressive behavior of the uncracked material is governed by the von-Mises failure criterion. When the stress state reaches the initial von Mises yield surface, the plastic behavior is represented by a J_2 -plasticity model. Between the initial yield surface and final failure surface, the material exhibits a strain-hardening behavior, followed by a strain-softening behavior after the final failure surface is reached. The von Mises criterion is expressed as

$$J_2 - \frac{1}{3}\sigma_e^2(\varepsilon_p) = 0 \quad (1)$$

in which J_2 is the second invariant of the deviatoric stress, σ_e is the effective stress, and ε_p is the effective plastic strain. For modeling the strain-hardening/softening behavior of concrete, the effective stress is expressed as a parabolic function of the effective plastic strain followed by an exponential function. As shown in Figure 2(a), this relation is defined by the following parameters: the compressive stress f_0 at first yielding, the compressive strength of the material f'_c , the strain at the peak stress ε_{1p} , and the strain ε_{2p} at the transition point between the parabola and the exponential function.

In tension, the material is initially linearly elastic and when the maximum principal stress reaches the tensile strength, cracks initiate in a direction normal to the direction of the maximum principal stress. The cracked material is considered as orthotropic with the axes of orthotropy, $n-t$, normal and tangential to the direction of the crack. In this study, the crack orientation and axes of orthotropy are assumed to remain constant. After cracking, the tensile stress decays exponentially as shown in Figure 2(b). Thus, the initial modulus of elasticity, E , tensile strength, f'_t , and a shape factor, α_1 , which controls the brittleness of the material, can define the tensile stress-strain relation.

The compressive stress-strain behavior for the cracked material is depicted in Figure 2(c), and is similar to the effective stress-strain relation of the plasticity model. It is parabolic with an exponential tail and is defined by the following three

parameters: the compressive strength of the material f'_c , the strain at the peak stress ε_1 , and the strain ε_2 at the transition point between the parabola and the exponential function.

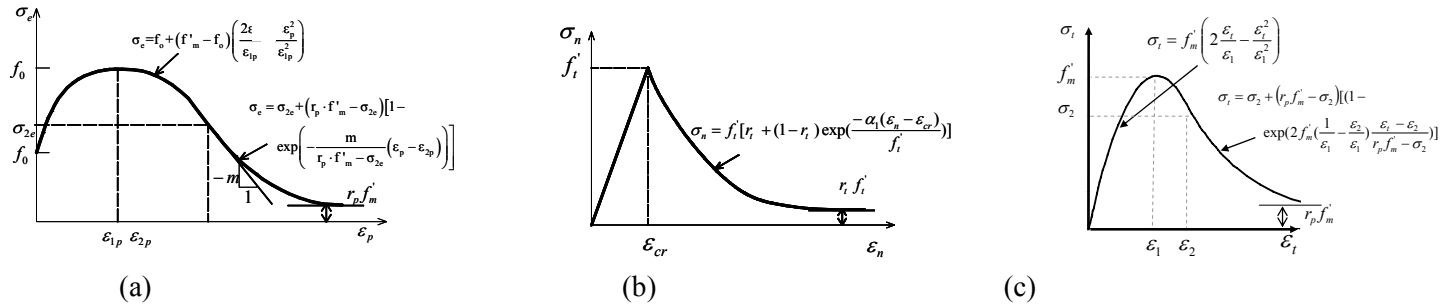


Figure 2: Smearing crack constitutive model: (a) effective stress-vs- effective plastic strain relation for J_2 plasticity model, (b) tensile behavior of orthotropic model, and (c) compressive behavior of orthotropic model.

4.2 Dilatant interface model

The interface model used in this study is implemented in FEAP as a 4-node, zero-thickness, isoparametric, line element. The model adopts a cohesive crack formulation that simulates mode-I, mode-II, and mixed-mode fracture (Lotfi and Shing 1994). It also accounts for the shear dilatation which can be important for simulating a confined crack. The model follows a classical elastic-plastic formulation.

$$\dot{\boldsymbol{\sigma}} = \mathbf{D}(\dot{\mathbf{d}} - \dot{\mathbf{d}}^p) \quad (2)$$

in which $\boldsymbol{\sigma} = \{\sigma \quad \tau\}^T$, with σ and τ being the normal and shear stresses at the interface, and $\mathbf{d} = \{d_n \quad d_t\}^T$, with d_n and d_t being the relative normal and shear displacements, the superposed dot represents the rate form, and \mathbf{D} is a diagonal matrix with elastic constants D_n and D_t .

The following hyperbolic yield surface is used to model fracture.

$$F(\boldsymbol{\sigma}, \mathbf{q}) = \tau^2 - \mu(\sigma - s)^2 + 2r(\sigma - s) = 0 \quad (3)$$

in which μ is the slope of the asymptotes of the hyperbola, s is the tensile strength, and r is the radius of the yield surface at the vertex of the hyperbola. The internal variables $\mathbf{q} = \{s \quad r \quad \mu\}^T$ control the evolution of the yield surface with $\mathbf{q}_0 = \{s_0 \quad r_0 \quad \mu_0\}^T$ characterizing the initial surface, while $\mathbf{q}_r = \{0 \quad r_r \quad \mu_r\}^T$ characterizes the final state. The following softening rules govern the evolution.

$$s = s_0 \left(1 - \frac{\kappa_1}{G_f^I} - \frac{\kappa_2}{G_f^{II}} \right) \geq 0, \quad r = r_r + (r_0 - r_r) e^{-\beta \kappa_3}, \quad \mu = \mu_r + (\mu_0 - \mu_r) e^{-\alpha \kappa_3} \quad (4)$$

in which G_f^I and G_f^{II} are the mode-I and mode-II fracture energies, α and β are material parameters controlling the rate of reduction of r and μ , and the κ_i 's represent the plastic work that governs the strength degradation. A non-associated flow rule with the following plastic potential is used.

$$Q(\sigma, q) = \eta \tau^2 + (r - r_r)(\sigma - s) \quad (5)$$

in which η is a scaling parameter controlling shear dilatation. The direction of plastic relative displacements is governed by the flow rule, i.e., $\dot{\mathbf{d}}^p = \lambda \frac{\partial Q}{\partial \boldsymbol{\sigma}} = \lambda \mathbf{m}$, where λ is the plastic multiplier. With the above plastic potential, the rate of shear dilatation decreases as the plastic work or the compressive stress increases.

5. CALIBRATION OF MATERIAL MODELS

5.1 Calibration of concrete model

In theory, one can obtain the tensile behavior of concrete with uniaxial tensile tests. However, these tests are generally difficult to conduct and indirect laboratory methods, such as the modulus of rupture and split cylinder tests, are often employed to extract the tensile strength. In the absence of tensile test data, concrete is normally considered linearly elastic before fracture, and its elastic modulus can be measured from compressive tests. Moreover, one can estimate the tensile strength of concrete from its compressive strength using empirical formulas available in design codes and the literature (MacGregor and Wight 2005). The post-peak tensile behavior can be determined with mode-I fracture tests, which are generally difficult to conduct. However, the mode-I fracture energy and, thereby, the post-peak behavior can be often estimated with test data and formulas available in the literature (e.g. Bazant and Becq-Giraudon 2002). Information on the mode-II (shear) fracture energy is more difficult to obtain. However, one can assume that $G_f^I = 10G_f^{II}$, which has been proven to provide satisfactory numerical results (Lotfi 1992).

The proposed modeling scheme proposed uses zero-thickness interface elements to capture dominant shear cracks in a concrete member in a more accurate manner. These elements are not supposed to influence the stiffness of the member before fracture. Therefore, their elastic stiffness should be high but not too high to make the model numerically ill-conditioned. Besides the tensile strength, the cohesive crack model used in this study allows one to specify the mode-I and mode-II fracture energies directly in terms of work per unit area. The fracture energies govern the evolution of the failure surface related to the fracture (de-cohesion) process. The change of the shape of the failure surface signifying the smoothening of a fractured interface under frictional work is governed by α and β , the material parameters controlling the rate of reduction of μ and r , respectively, as shown in equation 3. Information for the calibration of these parameters, as well as the dilatation parameter, η , is not readily available. Such properties depend on the size of aggregates, the composition of the mixture and other factors, and can be calibrated with mixed-mode fracture tests such as those conducted by Hassanzadeh (1990).

For the calibration of the tensile behavior of the smeared crack concrete elements, the calibrated stress-displacement curve of the interface model can be used as a reference. To match the tensile behavior of the smeared-crack and interface elements, one should consider the stress-displacement relations for the two types of elements. To define the appropriate stress-strain relation for a smeared crack element, one way is to determine the stress-displacement curve and relate strains to displacements by considering a characteristic length. For constant strain triangular elements, one can assume that the characteristic length be equal to the square root of the element area (Papadrakakis et al. 2005).

Furthermore, the smeared crack elements have to be calibrated to simulate the compressive behavior of concrete which is commonly obtained from compression tests of concrete cylinders. One can first calibrate the compressive stress-strain relation of the orthotropic model, and then calibrate the plasticity model accordingly to assure a smooth transition from the latter to the former at crack initiation. The compressive behavior of the elements should be calibrated with the consideration of the element size to avoid the mesh-size sensitivity problem (Bazant and Oh. 1983).

5.2 Calibration of masonry model

While a variety of tests are available to characterize the masonry materials (ASTM 2004), the calibration approach needs to consider the simplifying modeling assumptions. The zero-thickness interface elements used here to represent a mortar joint, as well as the two interfaces between the mortar and the bricks which are the weakest links in a masonry assembly. For the calibration of the shear behavior of the mortar joints, triplet tests or direct shear tests can be used. *In-situ* shove tests can be conducted to measure the shear strength and the corresponding normal load in a masonry wall. Results of such tests are reported by Van der Pliuym (1992), and Mehrabi et al. (1994).

Direct tensile tests on mortar joints are difficult to conduct and generally do not yield good results. However, the tensile strength of a brick-mortar interface can be obtained with beam tests or bond wrench tests. When shear test data is available, the mode-I fracture energy can be deduced from the mode-II fracture energy with the assumption that $G_f^I = 10G_f^{II}$. The Young's modulus of mortar can be determined with compression tests of mortar cylinders and the stiffness of the interface elements can be approximated as $D_n = E/h$, in which h is the height of the mortar joints in the specimen. Even though this assumption does not reflect the actual stiffness of a mortar joint as it ignores the confinement effect of the brick, the error can be compensated for by determining the brick element stiffness in such a way that the overall prism stiffness is matched.

The tensile and shear properties of the interface and smeared crack elements representing the brick can be calibrated in the same way as those simulating concrete. The tensile strength of the brick can be obtained with tensile splitting tests, while mode-I fracture tests can be used for the calibration of the post-peak behavior. Since mode-I fracture tests cannot be

easily conducted, experimental data available in literature can be used to estimate the mode-I fracture energy (Van der Pliujm 1992). However, one should be cautious about the possible differences in the geometry and material content of different bricks.

The smeared crack brick elements have to be so calibrated so that, combined with the mortar interface elements, they represent the compressive behavior of the masonry assembly. The interface element is elastic in compression and does not account for the Poisson effect of the mortar layer. To indirectly account for the 3-D brick-mortar interaction effect, the compressive behavior of the smeared crack elements modeling the brick should be calibrated with compression tests of masonry prisms rather than the compression tests of individual brick units.

6. EVALUATION OF THE MODELING SCHEME

6.1 Experimental models

The accuracy of the proposed modeling approach is evaluated with the consideration of two specimens tested by Mehrabi et al. (1994). They are Specimen 8, which was infilled with hollow concrete blocks (weak infill), and specimen 9, which had solid concrete bricks (strong infills). The frames were designed for moderate wind loads according to the provisions of ACI 318-89 and represented older structures that do not meet current seismic design requirements. Although the two specimens had the same detailing for the RC frames, as shown in Figure 3, their failure mechanisms were very distinct due to the different properties of the infill walls.

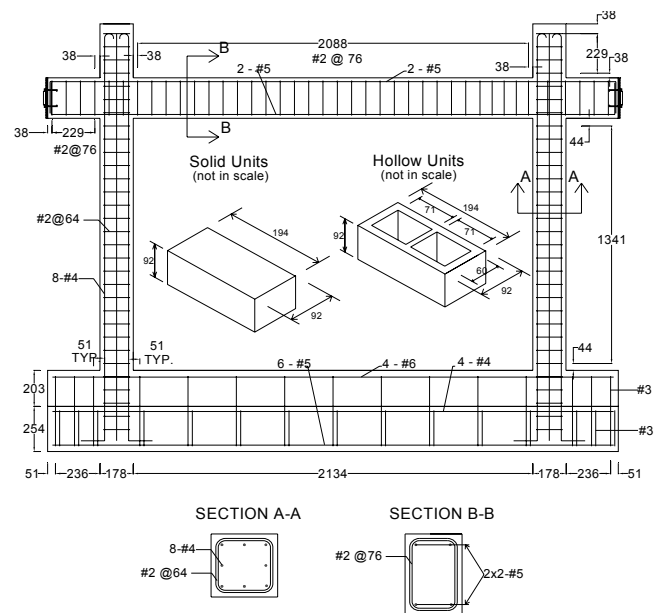


Figure 3: Design of reinforced concrete frame.

6.2 Numerical models

The infill and RC columns are modeled with the scheme shown in Figure 1. The base slab and the beam are modeled with 4-node smeared-crack elements only for computational efficiency since no dominant shear cracks are expected to develop. In the numerical model, the difference between the solid and hollow masonry units is reflected in the thickness and compressive behavior of the infill. The thickness of the infill in Specimen 8 is specified to be the total thickness of the face shells, which is 3.175 cm. The same concrete properties are assumed for Specimens 8 and 9 since the same RC frame was used. Thus, the damage and subsequent repair have not been accounted for in the modeling of Specimen 9.

The material models for concrete have been calibrated according to the proposed approach with data from compression and split cylinder tests conducted by Mehrabi et al. (1994). The calibrated models are shown in Figure 4(a) and (b). In lack of relevant experimental data, the post-peak tensile behavior of concrete is specified with the fracture energy values provided by Wittmann (2002). He obtained mode-I fracture energy ranges from 123 to 159 N/m for tensile strength values varying from 1.9 to 3.8 MPa. Split cylinder tests indicated a tensile strength of 2.76 MPa, hence, the mode-I fracture energy of the concrete is assumed to be 140 N/m.

The data from shear tests of mortar joints have been used to calibrate the interface elements in the masonry panel. The tests were conducted under constant compressive stresses of 345, 517, 689, and 1034 kPa, and yielded similar results for the hollow and solid concrete units. Mode-II fracture energy was determined by adjusting the analytical shear stress-shear displacement curve to match the experimental, and mode-I fracture energy was assumed to be 10 times larger. The experimental and analytical shear stress-shear displacement relations for a normal stress of 1034 kPa are shown in Figure 5(a). Figure 5(b) shows the peak and residual shear stress values observed in the tests and the yield and failure surfaces of the calibrated model. The initial tensile strength for the wall-to-beam and wall-to-column interfaces is assumed to be 1.38 kPa because these joints are normally weaker than the bed joints.

The compressive behavior of the masonry panel has been calibrated according to the proposed approach with prism test data conducted by Mehrabi et al (1994) and the material models are presented in Figure 4(a). The tensile strength of masonry units is assumed to be 10% of its compressive. For the mode-I fracture energy of the masonry units, Van der Pliujm (1992) has found values ranging from 60 to 130 N/m for tensile strength varying from 1.5 to 3.5 MPa. Therefore,

the mode-I fracture energy is assumed to be 105 N/m and the mode-II energy is calculated accordingly.

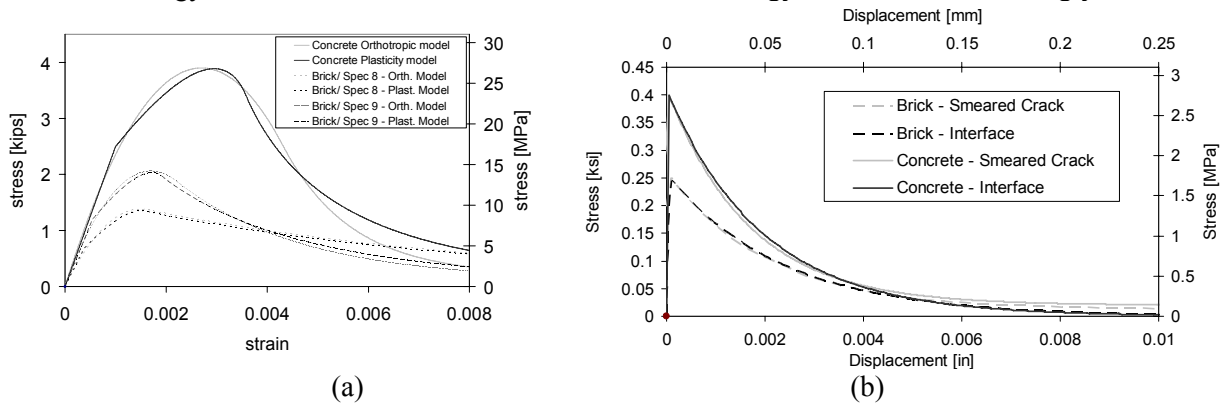


Figure 4: Calibration of smeared crack and interface models for concrete and brick: (a) compressive behavior and (b) tensile behavior.

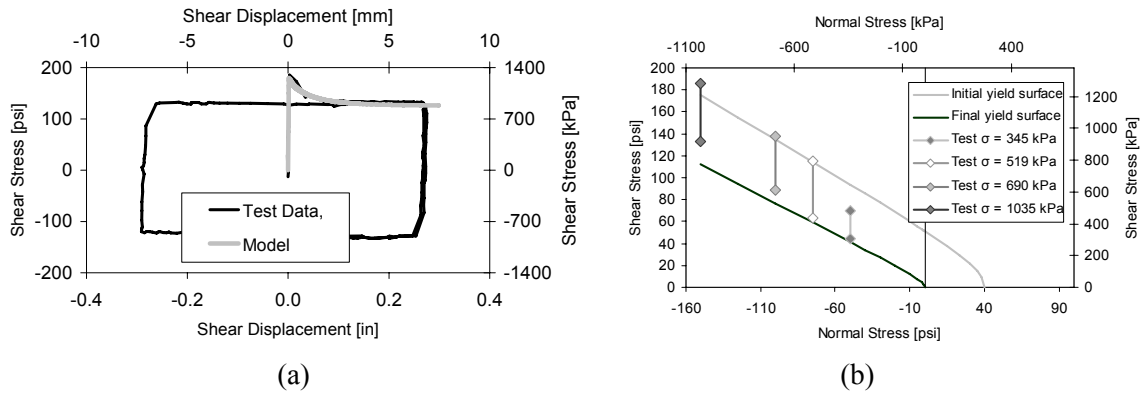


Figure 5: Calibration of interface model for mortar joints: (a) shear test and numerical results for $\sigma = 1034$ kPa (150 ksi) and (b) initial and final yield surfaces.

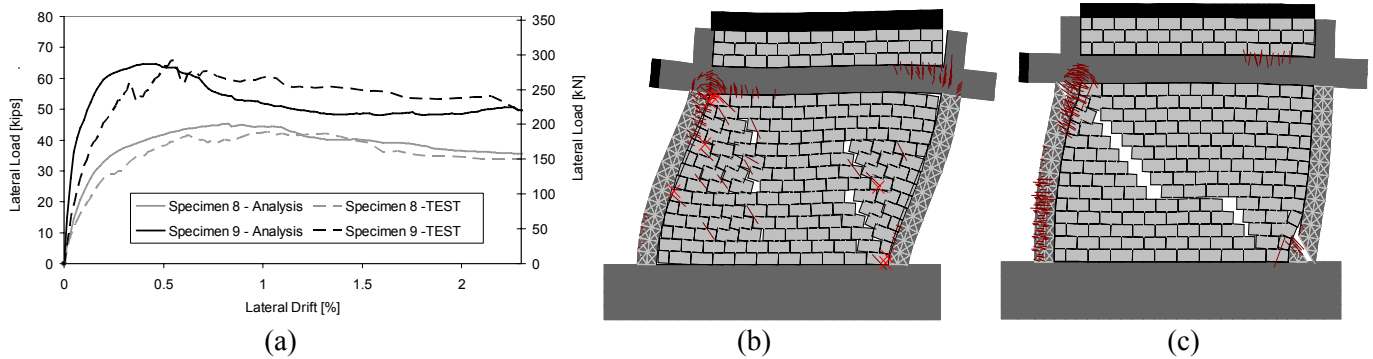


Figure 6: (a) Lateral force-Lateral displacement curves for experimental and computational models (b) Deformed mesh for Specimen 8 at lateral drifts peak load and lateral drift of 0.82%, (c) deformed mesh for Specimen 9 at peak load and lateral drifts of 0.46%.

6.3 Numerical results

The load-displacement relations obtained from the finite element models are compared with the experimentally obtained responses in Figure 6(a). The strength and post-peak behavior of the numerical models match the experimental results well. The numerical model for Specimen 8 captures well the experimentally measured initial stiffness but in the case of Specimen 9, it is overestimated. This is most likely caused by the fact that the model does not account for the pre-damage and repair of the RC frame.

The deformed mesh of Specimen 8 at the peak load is presented in Figure 6(b). The crushing of a smeared-crack element is denoted by an 'X', and cracking by a line reflecting the crack orientation. The length of each line corresponds to the

extent of crushing or crack opening. The failure pattern of the numerical model, resembles that of the physical specimen as it involves severe slip along a large number of bed joints and cracking and crushing of the masonry units and flexural behavior of the concrete columns.

The failure of Specimen 9 which included the strong infill initiated with the formation of a stair-stepped diagonal/sliding crack in the infill that was followed by a distinct diagonal shear crack at the top of the windward column. The shear-dominated failure sequence is accurately reproduced with the finite element model in terms of the load-vs-drift relation and the failure pattern that is illustrated in Figure 6(c).

7. SUMMARY AND CONCLUSIONS

This paper addresses the challenging issue of assessing the performance of existing masonry infilled RC frames under in-plane lateral loads. A finite element modeling methodology is developed, calibrated and validated with available experimental data. The proposed model combines the discrete and smeared crack approaches to circumvent the inadequacy of the smeared crack elements to simulate the brittle shear behavior of RC members and the mixed-mode fracture of masonry mortar joints. With the consistent calibration of this modeling approach, the distinct failure mechanisms of two frames infilled with strong and weak masonry, respectively, are successfully captured.

8. ACKNOWLEDGEMENTS

National Science Foundation Grant No. 0530709 supports the study presented in the paper under the George E. Brown, Jr. Network for Earthquake Engineering Simulation Research (NEESR) program. However, the opinions expressed in this paper are those of the authors and do not necessarily reflect those of the sponsor.

9. REFERENCES

- ASCE/SEI 41-06. (2006). "Seismic Rehabilitation of existing buildings.", ASCE, New York.
- Mehrabi, A. B., P. B. Shing, M. P. Schuller, and J. L. Noland (1994). Performance of masonry-infilled R/C frames under in-plane lateral loads. *Report No. CU/SR-94/6*, Univ. of Colorado, at Boulder.
- Lotfi, H. R. (1992). "Finite element analysis of fracture of concrete and masonry structures." Doctoral Dissertation, Univ. of Colorado at Boulder.
- Attard, M. M., A. Nappi, and F. Tin-Loi (2007). "Modeling fracture in Masonry." *J. Struct. Eng.*, ASCE, Vol. 133(10), 1385-1392.
- Al-Chaar, G. K., J. B. Berman, S. C. Sweeney (2003). "Investigation of FRP for seismic rehabilitation of RC structural frames with URM infill." *Report No. ERDC/CERL TR-03-10*, US Army Corps of Engineers.
- Fardis, M. N., S. N. Bousias, G. Franchioni, T. B. Panagiotakos (1999). "Seismic response and design of RC structures with plan-eccentric masonry infills." *J. Earthquake Eng. and Struct. Dyn.*, Vol. 28, 173-191.
- Bazant, Z.P and B.H. Oh (1983). "Crack Band theory for fracture of concrete". *Materials and Structures*, 31, RILEM, 16(93), 155-177.
- Lotfi, H. R. and P. B. Shing (1991). "An appraisal of smeared crack models for masonry shear wall analysis." *J. Computers Struct.*, ASCE, Vol. 120(1), 63-80.
- Taylor, R. L (2007). "FEAP - A Finite Element Analysis Program - Version 8.1." Dept. of Civil and Environmental Engineering, University of California at Berkeley, Berkeley, California.
- Lotfi, H. R. and P. B. Shing (1994). "An interface model applied to fracture of masonry structures". *J. Struct. Eng.*, ASCE, 120(1): 63-80.
- American Society for Testing and Materials. "Chemical-Resistant Nonmetallic Materials; Vitrified Clay Pipe; Concrete Pipe; Fiber-Reinforced Cement Products; Mortars and Grouts; Masonry; Precast Concrete". *ASTM Volume 04.05*, West Conshohocken, PA, 1997
- MacGregor, J. G, J. K. Wight (2005). "Reinforced Concrete Mechanics and Design." Pearson Prentice Hall, Upper Saddle River, NJ.
- Bazant Z. P., E. Becq-Giraudon (2002). Statistical prediction of fracture parameters of concrete and implications for choice of testing standard. *Cement and Concrete Research*, Elsevier, Vol. 32, 529-556.
- Hassanzadeh M., (1990). "Determination of fracture zone properties in mixed mode I and II." *J. Eng. Fracture Mechanics*. Col 35. No 4/5, 845-853.
- Papadrakakis M., V. Papadopoulos, M.Georgioudakis, Günter Hofstetter, Christian Feist. (2005) "Reliability analysis of a plain concrete beam", *IALAD Project Report*, Verbund - Austrian Hydro Power, Austria.
- Wittmann, F. H. (2002). "Crack formation and fracture energy of high strength concrete." *Sadhana*, Vol. 27, Part 4, 413-423.
- Pluijm, R. Van der (1992). "Material properties of masonry and its components under tension and shear." *6th Canadian Masonry Symposium*. Saskatchewan Canada: 675-686.